Original Research

# Construction of a Protocol for Measuring Blood Flow by Two-Dimensional Phase-Contrast MRA

Chris J.G. Bakker, PhD, Romhild M. Hoogeveen, MSc, Max A. Viergever, PhD

**Our aim is to describe and demonstrate the steps we have found to be useful in the construction and evaluation of protocols for triggered and nontriggered measurement of blood flow by two-dimensional phase-contrast magnetic resonance angiography (MRA). To achieve this goal, we start with a survey of factors governing the accuracy (validity) and precision (repeatability) of MR flow measurements. This knowledge, combined with prior information regarding the diameter of the target vessel and the prevailing flow conditions, is then employed to define a protocol for measuring flow with negligible systematic error. In the absence of a gold standard for in vivo flow measurements, the protocol is subsequently validated for a range of flow conditions by representative phantom experiments. Precision is then calculated from the signal-to-noise ratio (SNR) of blood in the accompanying magnitude images or, less conveniently, estimated from the standard deviation of repeated measurements. The desired precision is finally achieved by adjusting the appropriate SNR parameters. All steps involved in protocol development are demonstrated for both flow-independent and flow-dependent acquisitions. J. Magn. Reson. Imaging 1999;9:119–127.**


**Index terms:** magnetic resonance angiography; flow quantification; performance evaluation

IN PRESENT-DAY magnetic resonance (MR) practice, blood flow measurements are usually performed by two-dimensional phase-contrast MR angiography (MRA)(1). Applications have been reported throughout the vascular system, and major sources of error have been identified and discussed (2–4). To our knowledge, though, there is not much guidance in the literature as to how to construct and evaluate protocols for specific applications. It is the aim of our study to fill this gap by describing and demonstrating the steps we have discovered to be useful in developing protocols for quantitative assessment of undisturbed laminar blood flows. To achieve this goal, we start with a survey of factors governing the accuracy and precision of MR flow measurements. Here accuracy is taken to refer to the correctness of the result (validity, absence of systematic error), while precision is taken to describe how exactly the result is determined without reference to what the result actually means (repeatability, absence of random error). This knowledge, combined with prior information regarding the diameter of the target vessel and the prevailing flow conditions, will then be employed to define a protocol for measuring flow with negligible systematic error. In the absence of a gold standard for in vivo flow measurements, the protocol will subsequently be validated for a range of flow conditions by representative phantom experiments. Next, precision will be calculated from the signal-to-noise ratio (SNR) of blood in the accompanying magnitude images or, less conveniently, from the standard deviation of repeated measurements. The desired precision will finally be achieved by adjusting the appropriate SNR parameters. All steps involved in protocol development will be demonstrated for both nontriggered and triggered examinations and, as far as the latter type of flow measurement is concerned, for both flow-dependent and flow-independent acquisitions.

## SOURCES OF ERROR IN TWO-DIMENSIONAL PC FLOW MEASUREMENTS

MR flow measurements are usually performed by either triggered or nontriggered two-dimensional phase-contrast (two-dimensional PC) angiography. In the triggered mode (two-dimensional cine-PC), the flow rate is evaluated at various phases during the cardiac cycle, and the time-averaged flow rate, Q (mL/sec), is obtained by averaging across the resolved phases. In the nontriggered mode, temporal averaging is inherent to the measurement. This has the advantage that some of the errors in individual time measurements of flow velocity profile cancel by the time-averaging process (5). Nontriggered two-dimensional PC has been shown to produce valid results when flow is moderately pulsatile, a condition that is met, for instance, by the cranial circulation, and when acquisition parameters are chosen so as to make the signal of blood independent of its velocity (6–9). In this section we briefly summarize literature findings concerning the sources of systematic and random error for both types of flow measurement.

Department of Radiology, Image Sciences Institute, University Hospital Utrecht, 3584CX Utrecht, The Netherlands.

Address reprint requests to: C.J.G.B., Department of Radiology, University Hospital Utrecht, Heidelberglaan 100, 3584 CX Utrecht, The Netherlands. E-mail: C.J.G.Bakker@azu.rrn.nl

Received October 17, 1997; Accepted July 24, 1998.

### *Systematic Error in Triggered Two-Dimensional PC Flow Measurements*

#### *Partial Volume*

Owing to the limited spatial resolution of MR flow measurements, some of the voxels that cover the vessel lumen contain both flowing spins and stationary tissue. The resultant error in the calculated flow values is proportional to the relative number of edge voxels. Errors can be largely eliminated by increasing the spatial resolution so that the lumen contains at least 16 pixels (10), by decreasing the slice thickness, or by the application of a correction algorithm (11). Since partial volume errors essentially arise from the difference in signal magnitude between flowing blood and surrounding stationary tissue, errors can also be reduced by minimizing this difference, eg, by using small flip angles and short TEs, thus creating proton density contrast (4).

#### *Misalignment*

Misalignment between the flow-encoding axis and the flow direction increases partial volume errors and introduces smearing of the vessel because of flow displacement artifacts (12–14). Artifacts are particularly severe in regions with complex flow (15,16). Partial volume errors caused by misalignment can be suppressed by using thin slices, a high in-plane resolution, and proton-density weighted contrast. Displacement errors can further be reduced by selecting a straight vessel segment with laminar flow, by carefully positioning the scan plane normal to the flow streamlines, and by shortening the time between phase encoding and readout (strong gradients of short duration, short TEs).

#### *Higher Order Velocity Components*

The two-dimensional PC velocity-mapping technique is attuned to the quantification of linear motion. Results will therefore be degraded by higher order velocity components, eg, acceleration and jerk. According to recent studies (17,18), such errors can be minimized by encoding the velocity at the midpoint of the applied bipolar gradients and shortening TE.

#### *Intravoxel Phase Dispersion*

Two-dimensional PC velocity mapping assumes a symmetric distribution of velocity phase within a voxel. In case of asymmetry, the resultant intravoxel phase dispersion can be minimized by decreasing the velocity sensitivity of the experiment, i.e., increasing the encoded velocity, by diminishing the voxel size (19,20), and by shortening TE.

#### *Phase Offsets*

Phase errors, such as those caused by eddy currents or improperly balanced gradients, introduce spatially dependent offsets in the observed flow values. For a system with shielded gradients, eddy current effects are largely eliminated. The remaining errors can be corrected by measuring the phase offset in a region adjacent to the vessel of interest. Phase errors may also be introduced by partial echo sampling or half-matrix acquisition. These features should, therefore, be avoided, except when measuring complex flows. In that case, fractional echo sampling may outperform full echo sampling due to a significant reduction of TE-associated errors, eg, displacement artifacts (15,16).

#### *Aliasing*

Velocity aliasing occurs if the phase difference between the base images in two-dimensional PC exceeds the principal range $[-\pi,+\pi]$. To prevent aliasing, the encoded velocity (venc) should be set above the maximum velocity anticipated in the vessel of interest. It should be realized that aliasing is not always apparent in nontriggered measurements owing to the temporal averaging inherent in this type of measurement.

#### *ROI Size*

In deriving flow values from velocity images, attention should be paid to the proper positioning of the region of interest (ROI). For volumetric flow measurements, the ROI should encompass the entire lumen. Inclusion of surrounding stationary tissue voxels is not expected to affect accuracy, since such voxels do not carry flow. However, as pointed out in references 1 and 4 and discussed in the next section, precision will be adversely affected by increasing the ROI size.

### *Systematic Error in Nontriggered Two-Dimensional PC Flow Measurements*

#### *Amplitude and Phase Modulation Errors*

In addition to the above-mentioned sources of error, nontriggered measurements will be corrupted by amplitude and phase modulation errors. The severity of these errors depends on the pulsatility of the flow and on the choice of certain acquisition parameters (5,21). In previous phantom work (22), we have shown that it is possible to suppress amplitude effects by reducing the flip angle ($\alpha \leq 10°$) and the slice width, and to suppress phase modulation errors by decreasing the velocity sensitivity of the acquisition (venc well above vmax). In this way, valid results are obtained for stationary vessels with moderately pulsatile flow, such as those encountered in the cranial circulation, but with a strong penalty in precision (as will be discussed below).

#### *Ghost Artifacts*

In nontriggered acquisitions, pulsatile flow causes ghost artifacts in the phase-encoding direction. Assuming strictly periodic flow, linear phase-encoding order, and interleaved velocity encoding, the spacing between the ghosts, $\Delta y$ (mm), is given by (23):

$$\Delta y = 2 \times TR \times FOV_y \times f_h \times NSA \qquad (1)$$

where TR denotes the repetition time (seconds), $FOV_y$ the field of view in the phase-encoding direction (mm), $f_h$

the heart rate (Hz), and NSA the number of intraview signal averages [interview or serial averaging does not affect Δy (23)]. Parameters should, therefore, be chosen such that the spacing between the ghosts is larger than the diameter of the vessel of interest. The spacing should not be too large, however, since higher order ghosts may fold back onto the primary vessel. A special situation arises if NSA × TR equals the period of motion. In that case, ghost artifacts disappear since data collection is synchronized with the cardiac cycle. This has been termed pseudo-gating (24,25). Caution should also be exercised to avoid ghost interference from adjacent vessels. Appropriate orientation of the phase-encoding gradient is usually adequate for solving this problem. If not, presaturation can be considered. In general, ghost artifacts can be reduced by using small flip angles to suppress amplitude modulation, a low-velocity sensitivity to suppress phase modulation, and signal averaging to promote phase cancellation (26). In real life, ghost artifacts are never as simple, discrete, and localized as suggested by Eq. (1). Nevertheless adherence to the condition stated by this equation is recommended; violation yields disastrous results, even for perfectly regular flows.

### *Random Error in Triggered Two-Dimensional PC Flow Measurements*

*Noise*

In cardiac-triggered two-dimensional PC flow measurements, a velocity map is generated for each cardiac phase, q, by calculating the phase difference between two differently velocity-sensitized base images. One image, $S_{1q}$, is obtained from an experiment in which a bipolar gradient pulse is being used for encoding of flow in what one may arbitrarily refer to as the positive direction. The other image, $S_{2q}$, is obtained using an opposite bipolar gradient pulse. In the presence of noise, the complex signals $S_{1q}$ and $S_{2q}$ can be modeled by, respectively,

$$S_{1q} = A_{1q} \exp [1 (ø_{0q} + \Delta ø_q)] + N_{r1} + iN_{i1} \quad (2)$$

$$S_{2q} = A_{2q} \exp [i (ø_{0q} - \Delta ø_q)] + N_{r2} + iN_{i2} \quad (3)$$

In these expressions, $\Delta ø_q$ represents the additional phase associated with the encoding of flow in cardiac phase q, $ø_{0q}$ the incidental phase component, $A_{1q,2q}$ the respective signal magnitudes, and $N_{r1,2}$ and $N_{i1,2}$ the noise in the real and imaginary channels.

If we assume that the base images have equal magnitudes, i.e., $A_{1q} = A_{2q} = A_q$, and that the noise in the real and imaginary channels is uncorrelated and equal, and equal for both encodings, i.e., $E(N_{r1}) = E(N_{i1}) = E(N_{r2}) = E(N_{i2}) = s$, it can easily be shown (27) that the random error in the resultant velocity determinations, $\sigma_v$, is entirely determined by the velocity sensitivity of the experiment and the signal-to-noise ratio, $SNR_{p,q}$, of blood in the magnitude images:

$$\sigma_{v_{p,q}} = (\sqrt{2}/\pi).\ \text{venc.}\ s/A_{p,q} = (\sqrt{2}/\pi)\ .\ \text{venc}/SNR_{p,q} \quad (4)$$

In this expression, the indices p and q, respectively, account for the fact that the inflow conditions (and hence the signal magnitude) may vary from pixel to pixel and from cardiac phase to cardiac phase. Equation (4) is an articulation of the fact that noise in phase images is independent of the phase itself and is merely determined by the magnitude of the signal and hence the SNR of the magnitude image (28–30). Equation (4) implies that the absolute precision of velocity measurements for each cardiac phase and each location in the vessel can be controlled by either adjusting the velocity sensitivity of the experiment or by manipulating the experimental conditions that determine, respectively, the level of the noise ($B_0$, RF coil, field of view, scan matrix, slice thickness, number of signal averages, receiver bandwidth) and the magnitude of the blood signal in the base images (flip angle, TR, TE). Equation (4) further shows that, since the SNR of blood can be determined from the magnitude images, information with regard to precision can, in principle, be extracted from the measurement itself.

*ROI Size*

In applying Eq. (4), it should be realized that this equation describes the precision of the velocity measurement for individual pixels in all discerned cardiac phases. To calculate the time-averaged volumetric flow rate, Q, all pixels within the lumen must be added together, averaged across the resolved cardiac phases, and multiplied by the pixel size:

$$Q = \frac{1}{N_q} \sum_{p=1}^{N_p} \sum_{q=1}^{N_q} (dx\ dy\ v_{p,q}) \quad (5)$$

Here $v_{p,q}$ denotes the velocity (cm/sec) for the p-th pixel and q-th cardiac phase, $N_p$ the number of pixels in the ROI, $N_q$ the number of cardiac phases, and dxdy the pixel size ($cm^2$). Propagation of errors shows the resultant precision of the flow rate, $\sigma_Q$, to be determined by:

$$\sigma_Q = \frac{1}{N_q} dx\ dy \sqrt{\sum_{p=1}^{N_p} \sum_{q=1}^{N_q} (\sigma_{v_{p,q}})^2} \quad (6)$$

According to Eq. (4), this expression can be readily evaluated for a particular flow measurement by analyzing the accompanying magnitude images. Since the signal strength of blood may vary from pixel to pixel and from cardiac phase to cardiac phase, the result may be expected to exhibit a strong dependency on the flow conditions and on the parameters that govern inflow enhancement.

A simple situation arises if experimental conditions are such that inflow enhancement may be ignored, i.e., if the signal intensity of blood is made independent of the flow velocity. In that case, which can usually be accomplished by using small flip angles, $\sigma_v$ will become independent of spatial position and cardiac phase, and

Eq. (6) transforms into:

$$\sigma_Q = \frac{1}{\sqrt{N_q}} dx\ dy\ \sqrt{N_p}\ \sigma_v \qquad (7)$$

Equation (7) shows that integration across the ROI decreases absolute precision by a factor $\sqrt{N_p}$. Hence, ROIs should always be chosen to enclose the lumen as tightly as possible to maximize the absolute precision of flow measurements (1,4). A similar argument applies to the calculation of average luminal velocities, on the understanding that precision is now improved by $\sqrt{N_p}$ instead of decreased. Equation (7) also shows that averaging across cardiac phases improves precision by $\sqrt{N_q}$.

### *Random Error in Nontriggered Two-Dimensional PC Flow Measurements*

As discussed in a previous section, nontriggered measurements produce valid results only when flow is not too strongly pulsatile and when acquisition parameters are set to generate flow-independent contrast. Precision analysis is, therefore, very similar to the analysis presented for a triggered measurement with flow-independent contrast. The only difference is that, in nontriggered measurements, temporal averaging is inherent to the measurement. As a consequence, the precision by which the volumetric flow rate can be determined is given by:

$$\sigma_Q = dx\ dy\ \sqrt{N_p}\ \sigma_v \qquad (8)$$

By comparing Eqs. (7) and (8), it is readily appreciated that triggered and nontriggered measurements may be expected to produce identical results, in terms of precision, if the number of signal averages in the latter equals the number of resolved cardiac phases in the former, given otherwise identical sequence parameters. To put it differently: the precision of a nontriggered measurement (NSA = 1) may be expected to equal the precision per cardiac phase for a triggered measurement.

## CONSTRUCTION OF A PROTOCOL

Construction of a protocol for measuring blood flow involves a trade-off between parameters affecting accuracy and precision. As pointed out by Bevington (31), both must be considered in assessing the value of a measurement. Assuming periodic, pulsatile, laminar flow, accuracy will be largely determined by the voxel dimensions and the velocity sensitivity of the experiment. In general, accuracy can be improved by increasing the spatial resolution and the encoded velocity and by decreasing the contrast between flowing blood and surrounding tissue (3,4). Precision, on the other hand, is proportional to the SNR of blood in the magnitude images and the velocity sensitivity of the experiment. Precision is, therefore, likely to be adversely affected by measures that are taken to increase accuracy. Interestingly, the reverse is not necessarily true, at least for the regular flows considered here, i.e., precision may be improved by taking measures that do not degrade accuracy. Examples are the choice of a larger number of signal averages, the selection of a smaller receiver bandwidth, and the use of a coil with better SNR characteristics. Hence, it is convenient to start construction of a protocol with the elimination of systematic errors and deal with precision requirements afterwards.

As far as accuracy is concerned, it must be realized that there is no real gold standard for in vivo flow measurements. As a consequence, estimation of systematic error in clinical applications has to rely on phantom experiments rather than on a comparison with known values. With regard to precision, it should be noticed that precision can either be determined by repeating measurements or extracted from the SNR of blood in the magnitude images.

Taking into account the above considerations, activities involved in the construction of a protocol can be summarized as follows. First, the measurement task is described, i.e., a vessel of interest is selected and the desired precision of the measurement (reproducibility) is specified. Second, the experimental set-up is defined by selecting an MR scanner and the appropriate arrangement of RF transmit and receive coils. Third, prior knowledge regarding vessel size and flow conditions is used to define a protocol that is expected to produce negligible systematic error. Fourth, the protocol is validated by a representative set of phantom experiments, covering the range of flow conditions to be encountered in vivo. Fifth, precision is estimated from the SNR of blood in the accompanying magnitude images or by repeating measurements, and the proper SNR parameters are adjusted until the specified precision is achieved. Finally, the resultant protocol is tuned to other vessels of interest by adapting the spatial resolution, the velocity sensitivity, the SNR parameters, and the ROI size.

In the following discussion the efficacy of the indicated approach will be demonstrated for both nontriggered and triggered examinations.

## MATERIALS AND METHODS

Experiments were performed using a plastic tube with an inner diameter of 5.3 mm and a wall thickness of 0.1 mm. The tube was led through a reservoir with doped tap water and connected to a calibrated flow simulator (systematic error less than 1%) circulating blood mimicking fluid (Quest Image, London, Ontario). The fluid has a viscosity of 2.5 mPa.s, a density of 1.03 g/cm$^3$, a $T_1$ of about 650 msec (at 1.5 T), and a $T_2$ of about 350 msec (at 1.5 T). A vial with blood mimicking fluid was placed parallel to the tube to permit direct comparison between the imaging characteristics of stationary and flowing fluid and to allow estimation of residual phase errors. The system was set to generate weakly pulsatile flow with flow rates between 0 and 10 mL/sec and a cycle time of 960 msec, thus simulating the flow conditions normally encountered in the cerebral circulation (32). A typical waveform at the phantom as measured by two-dimensional cine-PC is shown in Fig. 1.

Measurements were performed with a 1.5 T system with shielded gradients (Gyroscan ACS/NT15, software

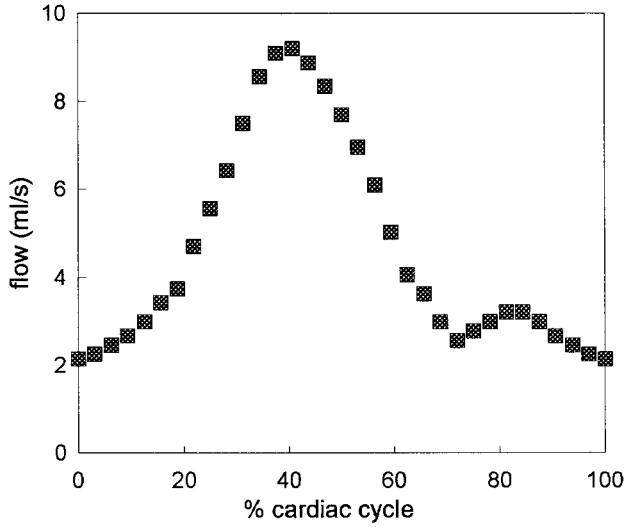


**Figure 1.** Typical waveform, i.e., flow rate (mL/sec) as a function of cardiac phase (%), at the phantom as measured by the two-dimensional cine-PC protocol from Table 1 (heart beat interval 960 msec, time-averaged flow rate 4.60 mL/sec).

release 4.5, Philips Medical Systems, Best, The Netherlands) using a body coil as transmitter and a quadrature head-neck coil as receiver. To illustrate the basic ideas behind the protocol development but to avoid excessive scan times, tests were initially carried out with nontriggered two-dimensional PC. Thus established procedures were subsequently applied to flow-independent and, finally, flow-dependent triggered examinations.

Nontriggered measurements were initially performed with the reference protocol of Table 1 (left column). Parameters were chosen largely to avoid systematic errors and to limit the duration of individual scans to about 30 seconds. According to Eq. (1), spacing between ghost images for this acquisition will be about 8 mm, large enough to prevent overlapping with the primary vessel image. Flow rates (mL/sec) were calculated by analyzing a fixed ROI of 50 $mm^2$ enclosing the vessel lumen. An ROI of equal size was used to analyze stationary fluid and to correct for offsets due to residual phase errors. Accuracy was estimated by comparing measured against known values. Precision was determined in two ways: first, by evaluating the SNR of blood in the magnitude images and using Eq. (8), and second, by calculating the standard deviation of repeated measurements ($n = 16$). The number of signal averages, the velocity sensitivity, the bandwidth, and the ROI size were adapted to attain the desired precision.

The same general procedure was applied for flow-independent triggered examinations, starting with the reference protocol of Table 1 (right column) with a flip angle of 7.5°. Precision was again determined by evaluating the SNR of blood in the magnitude images and using Eq. (7), and by repeating measurements ($n = 16$).

To study the effect of inflow enhancement on measurement precision in triggered acquisitions, the flip angle was varied between 7.5° and 90°. Precision was estimated from the SNR of blood in the magnitude images using Eq. (6). Since edge effects tend to become more severe with increasing flip angle, the ROI was restricted to the innermost 16 $mm^2$ of the vessel lumen in these calculations.

Table 1
Reference Protocols for Cardiac Triggered and Nontriggered Flow Measurements in a 5.3-mm-Diameter Stationary Vessel With Moderately Pulsatile Flow ($v_{max} < 200$ cm/sec)

| Scan parameter | Nontriggered | Triggered |
|---|---|---|
| Type of sequence | 2DPC | 2DPC |
| Repetition time (msec) | 15.0 | 15.0 |
| Echo time (msec) | 8.7 | 8.7 |
| Flip angle | 7.5° | 7.5°–90° |
| Cardiac triggering | No | Retrospective |
| Number of cardiac phases | — | 32 |
| Number of signal averages | 4 | 1 |
| Type of averaging | Serial | — |
| RF spoiling | Yes | Yes |
| Phase-encoding order | Linear | Linear |
| Partial echo sampling | No | No |
| Half-matrix acquisition | No | No |
| Scan plane orientation | Flow | Flow |
| Velocity encoding | Hadamard | Hadamard |
| Velocity sensitivity (cm/sec) | 200 | 200 |
| Receiver bandwidth (kHz) | 56 | 56 |
| Slice thickness (mm) | 8 | 8 |
| Field of view (mm) | 256 × 256 | 256 × 256 |
| Scan matrix | 256 × 256 | 256 × 256 |
| Reconstruction matrix | 256 × 256 | 256 × 256 |
| Image types | Velocity + magnitude | Velocity + magnitude |

## RESULTS

### *Nontriggered Measurement*

In a first set of experiments, accuracy and precision of two-dimensional PC flow measurements were evaluated by repeated calibration measurements ($n = 16$) with the nontriggered reference acquisition of Table 1. In these experiments flow was varied between 1 and 10 mL/sec. Table 2 shows the mean values, Q and $Q_0$, and the standard deviations, $\sigma_Q$ and $\sigma_{Q_0}$, of the observations for flowing and stationary blood mimicking fluid. Table 2 shows a systematic underestimation of the flow, $\delta Q$, of about 0.10 mL/sec on average and a random error, $\sigma_Q$, of 0.41 mL/sec on average. The offset is presumably caused by eddy currents and could in large part be corrected by subtracting the observed flow values, $Q_0$, for stationary fluid in the vial adjacent to the vessel under examination. Table 2 further shows that the repeatability of the measurements for flowing and stationary fluid on average are about equal, i.e., $\sigma_Q \approx \sigma_{Q_0}$. This confirms our anticipation, embodied by Eq. (8), that the precision of nontriggered measurements is largely independent of the flow itself and thus represents an absolute rather than a relative quantity. Taking into account ROI size, a random error of 0.41 mL/sec in the flow measurement can easily be shown to correspond to a precision of 5.8 cm/sec in the velocity determination for individual pixels [Eq. (8)]. According to Table 2, this is in good agreement with the $\sigma_v'$ and $\sigma_{v_0}'$ that are obtained by analyzing the SNR of flowing and stationary blood mimicking fluid in the magnitude images, SNR and $SNR_0$, respectively, and applying Eq. (4). In the SNR calculation, noise was approximated in the usual way, i.e., by taking the standard deviation of the

Table 2
Results of a Flow Calibration Experiment With Repeated Measurements ($n = 16$) Using the Reference Protocol of Table 1*

| $Q_{cal}$ (mL/sec) | Q (mL/sec) | $\delta Q$ (mL/sec) | $\sigma_Q$ (mL/sec) | $\sigma_v$ (cm/sec) | SNR | $\sigma_{v'}$ (cm/sec) | $Q_0$ (mL/sec) | $\sigma_{Q_0}$ (mL/sec) | $\sigma_{v_0}$ (cm/sec) | $SNR_0$ | $\sigma_{v'_0}$ (cm/sec) | $Q_{cor}$ (mL/sec) |
|---|---|---|---|---|---|---|---|---|---|---|---|---|
| 1 | 1.00 | 0.00 | 0.36 | 5.1 | 15.9 | 5.7 | −0.09 | 0.59 | 8.3 | 15.7 | 5.8 | 1.09 |
| 2 | 1.77 | −0.23 | 0.59 | 8.3 | 15.9 | 5.7 | −0.15 | 0.59 | 8.3 | 15.7 | 5.7 | 1.92 |
| 3 | 3.06 | 0.06 | 0.30 | 4.2 | 16.2 | 5.5 | −0.10 | 0.39 | 5.5 | 16.0 | 5.6 | 3.16 |
| 4 | 3.87 | −0.13 | 0.56 | 7.9 | 16.2 | 5.5 | −0.15 | 0.47 | 6.6 | 16.0 | 5.6 | 4.02 |
| 5 | 5.02 | 0.02 | 0.37 | 5.2 | 16.2 | 5.6 | −0.07 | 0.42 | 5.9 | 16.0 | 5.6 | 5.09 |
| 6 | 5.78 | −0.22 | 0.41 | 5.8 | 16.4 | 5.5 | −0.21 | 0.35 | 4.9 | 16.2 | 5.6 | 5.99 |
| 7 | 6.81 | −0.19 | 0.39 | 5.5 | 16.3 | 5.5 | −0.21 | 0.35 | 4.9 | 16.2 | 5.6 | 7.02 |
| 8 | 7.87 | −0.13 | 0.27 | 3.8 | 16.1 | 5.6 | −0.19 | 0.40 | 5.7 | 16.1 | 5.6 | 8.06 |
| 9 | 8.89 | −0.11 | 0.34 | 4.8 | 16.0 | 5.6 | −0.01 | 0.45 | 6.4 | 16.2 | 5.6 | 8.90 |
| 10 | 9.96 | −0.04 | 0.51 | 7.2 | 15.6 | 5.8 | −0.13 | 0.29 | 4.1 | 15.8 | 5.7 | 10.09 |
| | Mean | −0.10 | 0.41 | 5.8 | 16.1 | 5.6 | −0.13 | 0.43 | 6.1 | 16.0 | 5.6 | |

*$Q_{cal}$ = actual flow (1–10 mL/sec); Q = observed flow; $\delta_Q$ = difference between Q and $Q_{cal}$; $\sigma_Q$ = standard deviation ($n = 16$); $\sigma_v$ = precision of velocity determination per pixel as calculated from $\sigma_Q$ by applying Eq. (6); SNR = signal-to-noise ratio of flowing blood; $\sigma_{v'}$ = precision of velocity determination per pixel as calculated from SNR by applying Eq. (4); $Q_0$, $\sigma_{Q_0}$, $\sigma_{v_0}$, and $\sigma_{v'_0}$ represent the corresponding values for stationary blood mimicking fluid. The final column shows the corrected flow values, $Q_{cor} = Q - Q_0$.

background noise and dividing by 0.655 (33–35). Our observations thus demonstrate the flow-independent character of the acquisition and support our earlier assumption that the magnitude of the blood signal is virtually unaffected by the application of velocity-encoding gradients. The observations also confirm the fact stated by Eq. (4) that the precision of a flow measurement is governed by the SNR of blood in the magnitude images. As a consequence, precision can be directly estimated from the measurement itself and does not necessarily have to rely on repeated measurements.

According to the above experiments, the protocol of Table 1 yields negligible systematic errors and random errors of about 0.41 mL/sec when applied to a 5.3-mm-diameter vessel with moderately pulsatile flow between 0 and 10 mL/sec. In theory, a specified precision can now be achieved by adapting the appropriate scan parameters. To demonstrate this experimentally, a set of experiments was performed in which precision was studied as a function of encoded velocity (venc), number of signal averages (NSA), matrix size, and trigger mode. In these experiments, the average flow was kept at 4.60 mL/sec, while measurements were repeated 16 times (occasionally 64 times) and evaluated by analyzing a 50 $mm^2$ ROI. Unless stated otherwise, scan parameters were chosen as specified in Table 1.

Table 3 shows the mean values, Q and $Q_0$, and the standard deviations, $\sigma_Q$ and $\sigma_{Q_0}$, of the observations for flowing and stationary blood mimicking fluid. Again, observed flow values are slightly low, while the precision of corresponding measurements for flowing and stationary fluid on average is about equal. Table 3 further largely confirms the predicted effects of parameter changes on measurement precision. An increase in the number of signal averages, for instance, improves precision by a factor that is about proportional to the square root of the NSA. This is also demonstrated by Figs. 2 and 3, which, respectively, display vessel and background flow values for 64 consecutive measurements with NSA = 1 and 16 measurements with NSA = 16. Table 3 further confirms that an increase in the venc invokes a proportional degradation of the precision. Interpretation of the effect of the scan matrix is slightly more

Table 3
Results of an Experiment in Which the Accuracy and Precision of Flow Measurements Were Determined as a Function of the Number of Signal Averages (NSA), the Velocity Sensitivity (Venc), the Scan Matrix (Matrix), and the Trigger Mode (ECG)*

| NSA | VENC (cm/sec) | Matrix | TE (msec) | BW Hz/pix | $N_p$ | Q (mL/sec) | $\sigma_Q$ (mL/sec) | $Q_0$ (mL/sec) | $\sigma_{Q_0}$ (mL/sec) | $Q_{cor}$ (mL/sec) |
|---|---|---|---|---|---|---|---|---|---|---|
| 1 | 200 | 256 | 8.7 | 220 | 50 | 4.49 | 0.81 | −0.08 | 0.86 | 4.57 |
| 2 | 200 | 256 | 8.7 | 220 | 50 | 4.57 | 0.65 | −0.29 | 0.53 | 4.86 |
| 4 | 200 | 256 | 8.7 | 220 | 50 | 4.42 | 0.42 | −0.09 | 0.36 | 4.51 |
| 8 | 200 | 256 | 8.7 | 220 | 50 | 4.53 | 0.33 | −0.03 | 0.27 | 4.56 |
| 16 | 200 | 256 | 8.7 | 220 | 50 | 4.58 | 0.22 | −0.06 | 0.22 | 4.64 |
| 4 | 100 | 256 | 8.7 | 220 | 50 | 4.51 | 0.25 | −0.10 | 0.24 | 4.61 |
| 4 | 200 | 256 | 8.7 | 220 | 50 | 4.49 | 0.34 | −0.26 | 0.47 | 4.75 |
| 4 | 300 | 256 | 8.7 | 220 | 50 | 4.63 | 0.61 | −0.03 | 0.51 | 4.66 |
| 4 | 400 | 256 | 8.7 | 220 | 50 | 4.50 | 0.71 | −0.07 | 0.85 | 4.57 |
| 4 | 200 | 512 | 15.0 | 110 | 200 | 4.61 | 0.35 | −0.03 | 0.44 | 4.64 |
| 4 | 200 | 256 | 15.0 | 220 | 50 | 4.48 | 0.43 | −0.03 | 0.37 | 4.51 |
| 4 | 200 | 128 | 15.0 | 440 | 16 | 4.56 | 0.41 | −0.03 | 0.47 | 4.59 |
| 32 (ECG) | 200 | 256 | 8.7 | 220 | 50 | 4.47 | 0.16 | −0.10 | 0.13 | 4.57 |

*Variation of the scan matrix was accompanied by the indicated modifications of the bandwidth per pixel (BW), echo time (TE), and number of pixels within the region of interest ($N_p$). Flow was weakly pulsatile, with an average flow rate of 4.60 mL/sec. Values represent mean values and standard deviations of 16 measurements. Q = observed flow; $\sigma_Q$ = standard deviation ($n = 16$); $Q_0$ and $\sigma_{Q_0}$ represent the corresponding values for stationary blood mimicking fluid; the final column shows the corrected flow values, $Q_{cor} = Q - Q_0$.

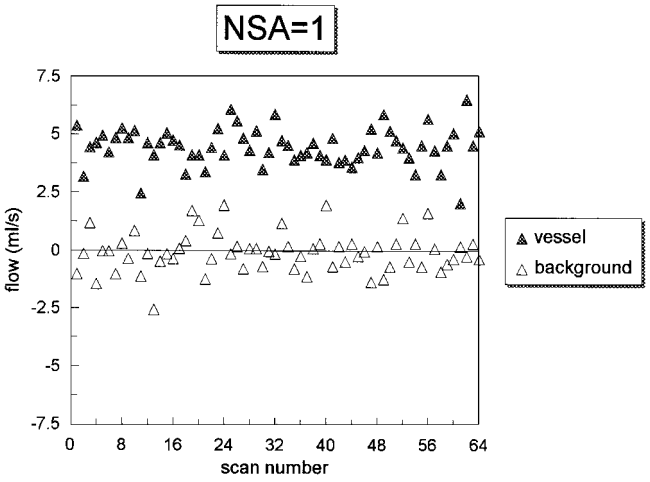


**Figure 2.** Consecutive flow measurements ($n$ = 64) with NSA = 1 in a 5.3-mm-diameter vessel with pulsatile flow (waveform as displayed in Fig. 1, time-averaged flow rate 4.60 mL/sec).

complex. For a fair assessment, the echo time was fixed at 15 msec in these experiments, the minimum TE for a 512 matrix. Since the receiver bandwidth was kept at 56 kHz, the bandwidth per pixel is dependent on the matrix size. As a consequence, doubling of the matrix will halve the SNR. At the same time, however, the number of pixels in the ROI will be quadrupled by the increase in spatial resolution. According to Eqs. (4) and (8), the overall effect on measurement precision will, therefore, be negligible. A similar argument applies when the scan matrix is halved. The predicted behavior of $\sigma_Q$ and $\sigma_{Q_0}$ is nicely confirmed by Table 3, especially if it is realized that the error in the standard deviation as determined from $n$ = 16 measurements is still about 18%.

### *Flow-Independent Triggered Measurement*

To demonstrate the effect of cardiac triggering (ECG) on measurement precision, triggered measurements were initially performed with the same sequence parameters as the nontriggered measurements (Table 1), i.e., the flip angle was set at 7.5° to generate flow-independent magnitude images. Values represented in Table 3 were obtained by integrating across a 50 mm$^2$ ROI and averaging across all 32 heart phases fitting into the 960 msec RR interval (ECG 32). Table 3 makes a reasonable case for our anticipation that the precision of the triggered acquisition is about equal to the precision of a nontriggered measurement with NSA = 32. This is an obvious result if it is appreciated that the SNR of blood in the magnitude images, and hence precision is virtually independent of cardiac phase and spatial position for the employed acquisition. Table 3 also shows good agreement between the precision as determined from Eq. (7) and by repeating measurements.

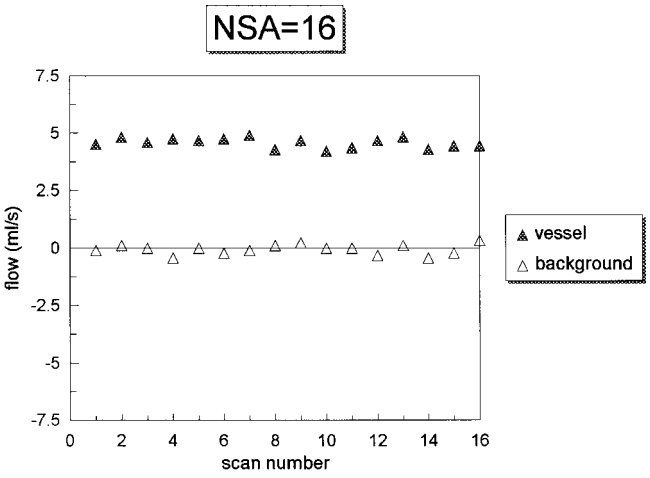


**Figure 3.** Consecutive flow measurements ($n$ = 16) with NSA = 16 in a 5.3-mm diameter vessel with pulsatile flow (waveform as displayed in Fig. 1, time-averaged flow rate 4.60 mL/sec).

### *Flow-Dependent Triggered Measurement*

To study the effect of inflow enhancement on measurement precision in triggered examinations, the flip angle was varied between 7.5° and 90°. Figure 4 shows the precision as a function of flip angle and cardiac phase for pulsatile flow with a flow rate of 4.6 mL/sec (Fig. 1). Precision was calculated by Eq. (6), using an ROI of 16 mm$^2$. The observed behavior in Fig. 4 is explained by two mechanisms: inflow enhancement and saturation by repetitive excitations. The balance between both will depend on the flow and the flip angle. This is illustrated by Fig. 5 for flow rates of 0.0, 2.3, 4.6, and 6.9 mL/sec. For stationary blood, optimum precision is achieved at

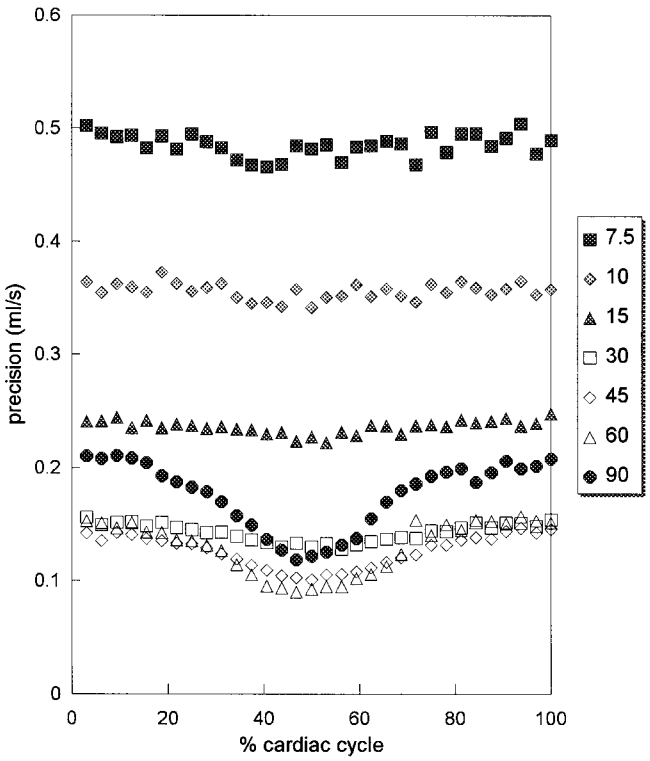


**Figure 4.** Precision of the flow rate, $\sigma_Q$ (mL/sec), as a function of cardiac phase (% of cardiac cycle) for a triggered measurement with various flip angles and other scan parameters as described in Table 1. Measurements were performed in a 5.3-mm-diameter vessel with pulsatile flow (waveform as displayed in Fig. 1, time-averaged flow rate 4.60 mL/sec). Precision was calculated for an ROI of 16 mm$^2$.

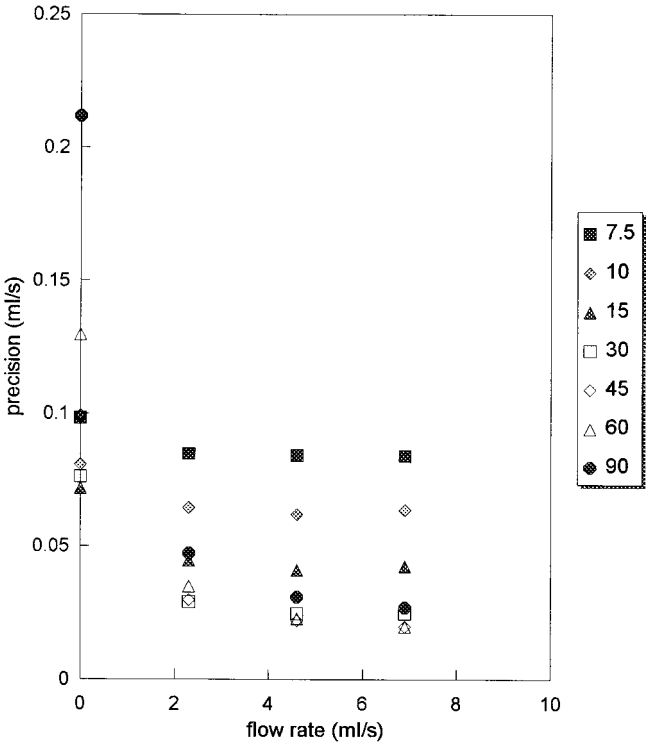


**Figure 5.** Precision of the time-averaged flow rate, $\sigma_Q$ (mL/sec), as a function of the flow rate (mL/sec) for a triggered measurement with various flip angles and other scan parameters as described in Table 1. Measurements were performed in a 5.3-mm diameter vessel with pulsatile flow (waveform as displayed in Fig. 1, time-averaged flow rates of 0.00, 2.30, 4.60, and 6.90 mL/sec).

about 15°. For higher flow rates and hence more prominent inflow enhancement, the optimum shifts to larger flip angles. A flip angle of 30° appears to be about optimum for the considered range of flow values, the more so since, for larger flip angles, magnitude and velocity images were found to be increasingly corrupted by ringing artifacts. These artifacts are caused by the extreme contrast between vessel and background that occurs for larger flip angles (36) and make the estimated flow values strongly dependent on the placement of the ROI. According to Fig. 5, a flip angle of 30° yields a gain in precision of a factor of about 3 compared with a flow-independent examination (flip angle 7.5°). The gain was found to be somewhat less, however, if the ROI was enlarged so as to include the slowly flowing blood near the vessel walls and, inadvertently, some surrounding stationary tissue. As explained above, calculations for larger ROIs tended to be corrupted by ringing artifacts.

## DISCUSSION

To demonstrate the steps involved in the construction of a protocol, flow measurements were performed in a 5.3-mm-diameter vessel exhibiting undisturbed pulsatile laminar flow. This was done with a reference protocol in which the acquisition parameters were chosen so as to avoid systematic errors. The absence of systematic errors was confirmed by calibration experiments. A specified precision was achieved by adapting the appropriate SNR parameters.

The reported phantom experiments show that, at least for the simple flow conditions considered here, protocols can be attuned to the needs of specific applications by selecting the appropriate spatial resolution, velocity sensitivity, trigger mode, and SNR parameters of the acquisition. According to our findings, this adaptation does not require any further experimentation as long as the set-up remains unchanged and current knowledge about the control of systematic errors is observed. This implies that the effectivity of a protocol for a certain task can be assessed prospectively if some prior information with regard to vessel dimensions and flow conditions is available.

In considering application of the principles described to clinical flow measurements, one must realize that there is no real gold standard for in vivo measurements. As a consequence, estimation of systematic error in clinical measurements has to rely on representative phantom experiments rather than on a comparison with known values. As far as precision (repeatability) is concerned, one must recognize that biological variation constitutes an additional source of random error in in vivo measurements. This is especially true if the measurement is not synchronized to the cardiac cycle, as is the case with nontriggered measurements. However, it has been shown that this source of variation is largely eliminated by extending the measurement across at least 20 heart cycles (37), a condition that is amply met by our reference protocol. Another point of concern in nontriggered measurements is that scan conditions must be chosen so as to avoid ghost artifacts that overlap on the original vessel.

It should be noted that most of our results were obtained with flow-independent nontriggered and triggered two-dimensional PC sequences, featuring a repetition time of 15 msec, an echo time of 8.7 msec, and a flip angle of 7.5°. The use of nontriggered acquisitions was motivated by our intent to simplify the analysis and to keep examination time for repeated acquisitions within acceptable limits. Besides, nontriggered measurements are increasingly employed in clinical studies (6–9) and deserve some attention on that account. Unfortunately, the small flip angles inherent in nontriggered measurements imply a loss in precision by discarding inflow effects. According to our experiments with flow-independent and flow-dependent triggered acquisitions, a two- to threefold increase in precision may be anticipated by using a flip angle of 30° instead of 7.5°.

It should be emphasized that precision values reported in this in vitro study do not necessarily apply to the in vivo situation for several reasons. First, the blood mimicking fluid used in our study is an imperfect substitute for human blood. Second, the programmable flow pump applied introduces some additional noise in the images. Third, the noise level is dependent on the object. In our view, this does not detract from the value of the proposed guidelines for protocol development for the in vivo situation, since the factors mentioned all relate to measurement precision, and since precision, other than accuracy, does not rely on in vitro experiments but can be determined in vivo directly.

Finally, it must be stressed that the proposed guidelines for protocol development are only valid for the flow conditions modeled by the phantom experiments, i.e.,

periodic, pulsatile, laminar flow. For these conditions, often encountered in the normal circulation, systematic errors well below 5% can readily be achieved by controlling partial volume and displacement errors (sufficient spatial resolution, scan plane normal to streamlines, minimum contrast between blood and surrounding tissue), higher order phase errors (short TEs, velocity encoding at midpoint of bipolar gardients), intravoxel phase dispersion (small voxels, short TEs), ringing effects (moderate flip angles), aliasing (adequate velocity sensitivity), and ghost overlaps (intraview averaging, TR). This has been demonstrated for steady and pulsatile flows by many investigators including ourselves (22) using protocols similar to those displayed in Table 1.

In clinical applications, the phantom protocols may only be expected to produce equally accurate results for similar flow conditions and vessel geometries. Measurements should, therefore, be performed in fairly straight vessel segments with laminar flow. For complex flows and geometries (bends, bifurcations, stenotic regions, etc.), nonstationary vessels, and highly irregular cardiac cycles, artifacts are much less predictable, and general guidelines will be hard to construct. Hardware and software improvements, extensive simulation studies, and phantom experiments will be required to achieve command of this area.

## CONCLUSIONS

A protocol for unbiased measurement of undisturbed pulsatile laminar flow can be constructed by observing published findings concerning systematic error in two-dimensional PC flow measurements. A specified precision can be achieved by a conscious choice of the SNR parameters of the experiment.

## REFERENCES


1. Pelc NJ, Herfkens RJ, Shimakawa A, Enzmann DR. Phase contrast cine magnetic resonance imaging. Magn Reson Q 1991;7:229–254.
2. Bogren HG, Buonocore MH. Blood flow measurements in the aorta and major arteries with MR velocity mapping. J Magn Reson Imaging 1994;4:119–130.
3. Buonocore MH, Bogren H. Factors influencing the accuracy and precision of velocity-encoded phase imaging. Magn Reson Med 1992;26:141–154.
4. Wolf RL, Ehman RL, Riederer SJ, Rossman PJ. Analysis of systematic and random error in MR volumetric flow measurements. Magn Reson Med 1993;30:82–91.
5. Hangiandreou NJ, Rossman PJ, Riederer SJ. Analysis of MR phase-contrast measurements of pulsatile velocity waveforms. J Magn Reson Imaging 1993;3:387–394.
6. Tarnawski M, Padayachee S, West DJ, et al. The measurement of time-averaged flow by magnetic resonance imaging using continuous acquisition in the carotid arteries and its comparison with Doppler ultrasound. Clin Phys Physiol Meas 1990;11:27–36.
7. Enzmann DR, Marks MP, Pelc NJ. Comparison of cerebral artery blood flow measurements with triggered cine and non-triggered 2D phase-contrast techniques. J Magn Reson Imaging 1993;3:705–712.
8. Jordan JE, Pelc NJ, Enzmann DR. Velocity and flow quantification in the superior sagittal sinus with ungated and cine (gated) phase-contrast MR imaging. J Magn Reson Imaging 1994;4:25–28.
9. Bakker CJG, Hartkamp MJ, Mali WPTM. Measuring blood flow by nontriggered 2D phase-contrast MR angiography. Magn Reson Imaging 1996;14:609–614.
10. Tang C, Blatter DD, Parker DL. Accuracy of phase-contrast flow measurements in the presence of partial-volume effects. J Magn Reson Imaging 1993;3:377–385.
11. Hamilton CA. Correction of partial volume inaccuracies in quantitative phase contrast MR angiography. Magn Reson Imaging 1994;12: 1127–1130.
12. Von Schulthess GK, Higgins CB. Blood flow imaging with MR: spin-phase phenomena. Radiology 1985;157:687–695.
13. Firmin DN, Nayler GL, Kilner PJ, Longmore DB. The application of phase shifts in NMR for flow measurements. Magn Reson Med 1990;14:230–241.
14. Nishimura DG, Jackson JI, Pauly JM. On the nature and reduction of the displacement artifact in flow images. Magn Reson Med 1991;22:481–492.
15. Frayne R, Rutt BK. Understanding acceleration-induced displacement artifacts in phase-contrast MR velocity measurements. J Magn Reson Imaging 1995;5:207–215.
16. Steinman DA, Ross Ethier C, Rutt BK. Combined analysis of spatial and velocity displacement artifacts in phase contrast measurements of complex flows. J Magn Reson Imaging 1997;7:339–346.
17. Oshinski JN, Ku DN, Bohning DE, Pettigrew RI. Effects of acceleration on the accuracy of MR phase velocity measurements. J Magn Reson Imaging 1992;2:665–670.
18. Kouwenhoven M, Hofman MBM, Sprenger M. Motion induced phase shifts in MR: acceleration effects in quantitative flow measurements, a reconsideration. Magn Reson Med 1995;33:766–777.
19. Hamilton CA, Moran PR, Santago P, Rajala SA. Effects of intravoxel velocity distributions on the accuracy of the phase-mapping method in phase-contrast MR angiography. J Magn Reson Imaging 1994;4: 752–755.
20. Urchuk S, Plewes D. Mechanisms of flow-induced signal loss in MR angiography. J Magn Reson Imaging 1992;2:453–462.
21. Hofman MBM, Kouwenhoven M, Sprenger M, Van Rossum AC, Valk J, Westerhof N. Nontriggered magnetic resonance velocity measurement of the time-average of pulsatile velocity. Magn Reson Med 1993;29:648–655.
22. Bakker CJG, Kouwenhoven M, Hartkamp MJ, Hoogeveen RM, Mali WPTM. Accuracy and precision of time-averaged flow as measured by non-triggered 2D phase-contrast MR angiography: a phantom study. Magn Reson Imaging 1995;13:959–965.
23. Wood ML, Henkelman RM. MR image artifacts from periodic motion. Med Phys 1985;12:143–151.
24. Haacke EM, Lenz GW, Nelson AD. Pseudo gating: elimination of periodic motion artifacts in magnetic resonance imaging without gating. Magn Reson Med 1987;4:162–174.
25. Dixon WT, Brummer ME, Malko JA. Acquisition order and motional artifact reduction in spin warp images. Magn Reson Med 1988; 6:74–83.
26. Wood ML, Henkelman RM. Suppression of respiratory motion artifacts in magnetic resonance imaging. Med Phys 1986;13:794–805.
27. Andersen AH, Kirsch JE. Analysis of noise in phase contrast MR imaging. Med Phys 1996;23:857–868.
28. Conturo TE, Smith GD. Signal-to-noise in phase angle reconstruction: dynamic range extension using phase reference offsets. Magn Reson Med 1990;15:420–437.
29. Bernstein MA, Ikezaki Y. Comparison of phase-difference and complex-difference processing in phase-contrast MR angiography. Magn Reson Imaging 1991;10:725–729.
30. Lee AT, Pike GB, Pelc NJ. Three-point phase-contrast velocity measurements with increased velocity-to-noise ratio. Magn Reson Med 1995;33:122–125.
31. Bevington PR. Data reduction and error analysis for the physical sciences. New York: McGraw-Hill; 1969.
32. Enzmann DR, Ross MR, Marks MP, Pelc NJ. Blood flow in major cerebral arteries measured by phase-contrast cine MR. AJNR 1994;15:123–129.
33. Edelstein WA, Bottomley PA, Pfeifer LM. A signal-to-noise calibration procedure for NMR imaging systems. Med Phys 1984;11:180–185.
34. Henkelman RM. Measurement of signal intensities in the presence of noise in MR images. Med Phys 1985;12:232–233.
35. McGibney G, Smith MR. An unbiased signal-to-noise ratio measure for magnetic resonance images. Med Phys 1993;20:1077–1078.
36. Czervionke LF, Czervionke JM, Daniels DL, Haughton VM. Characteristic features of MR truncation artifacts. AJNR 1988;9:815–824.
37. Cloutier G, Allard L, Guo Z, Durand LG. The effect of averaging cardiac Doppler spectrograms on the reduction of their amplitude variability. Med Biol Eng Comput 1992;30:177–186.